Second order division in sectors as a prepattern for sensory organs in vertebrate development

Vincent Fleury, Alexis Peaucelle, Anick Abourachid, Olivia Plateau

Second order division in sectors as a prepattern for sensory organs in vertebrate development

Vincent Fleury[1], Alexis Peaucelle[2], Anick Abourachid[3] and Olivia Plateau[1,3,4]

[1]Laboratoire Matière et Systèmes Complexes, UMR 7057 Université de Paris/CNRS, 10 rue Alice Domont et Léonie Duquet, 75013 Paris, France.

[2]Institut Jean-Pierre Bourgin, UMR 1318 INRA/CNRS
INRA Centre de Versailles-Grignon
Route de St-Cyr (RD10), 78026 Versailles Cedex, France.

[3]Laboratoire Mécanismes Adaptatifs et Evolution, UMR 7179 MNHN/CNRS, CP 55, 57 rue Cuvier 75231 Paris cedex 05, France.

[4]Département de Géosciences, Université de Fribourg,
Ch. du Musée 6, 1700 Fribourg, CH

Abstract.

We describe a general biophysical mechanism underlying sensory organ formation. We show that the early vertebrate embryo, presents a principal structure made out of concentric rings and a secondary structure composed of radial sectors. During development, physical forces deform the main rings into axially directed, antero-posterior tubes, while the sectors roll up to form cylinders that are perpendicular to the antero-posterior axis. As a consequence, the basic structure of a vertebrate is a series of encased antero-posterior tubes (gut, neural tube, body envelope, amnion, chorion) decorated with smaller orifices (ear duct, eye stalk, nasal duct, gills) forming at right angles to the main body axis. We argue that the second order divisions reflect the early pattern of cell cleavage.

I. Introduction

What are the physical determinants and constraints of animal formation is an important question that complements the genetic and biochemical aspects of embryo development. Inside a given animal phylum, the formation of gross anatomical traits is universal, despite considerable variations in the genetic material from one species to another. In vertebrates, the early embryonic pattern is common to all taxa [1], with only minor variations. From the primitive lamprey all the way to mammals, the vertebrate taxa exhibit a recognizable pattern composed of a roughly cylindrical body elongated along the Antero-Posterior (AP) axis and a series of orifices perpendicular to the main body axis (Fig. 1A), and located at the boundary beween the ventral and dorsal parts of the animal (the Dorso-Ventral (DV) boundary). These orifices comprise the eyes, the nasal and otic pits and the mouth. In amniotes and mammals, head flexure complicates the matter and influences organ shape [2]. The embryonic precursors of these organs are called placodes [3]. Chondrichthyan vertebrates such as the sharks or rays[1] display slit-like orifices, like gills, but in a similar regular pattern (Fig. 1B, C). The question we address in this report is that of the role of mechanical constraints in the genesis of sensory organs. What is the topological origin of placodes and why do they transform into sensory organs in some taxa, and in slits or even jaws (Fig. 1D) in others? We rely on time-Lapse (T-L) video microscopy of the developing chicken embryo to elaborate a fundamental physical model of sensory organ formation in this vertebrate. Our model allows us to determine mathematically how formation of the mouth and sensory organs along the body wall occurs.

We first recall how the main AP directed tubes (neural tube, body wall, aminiotic sac etc.) form in a vertebrate. After fertilization, the first cleavages generate a concentric ring structure [4]. Cell size varies stepwise from one ring to the next (Fig. 2A). This creates a contrast of mechanical properties between the rings [5]. This contrast localizes the boundaries between body parts by a robust mechanism of fold-locking at lines of elastic discontinuity [5-7]. The main driving forces are initially distributed along the very same concentric rings [8-12]. These rings are skewed posteriorly, due to the additional AP asymmetry of the embryo[2]. This encased ring pattern contracts sequentially because the constrictions are excitable, just as a muscular reflex [13]. The main AP body features of vertebrate embryos is therefore an attractor of a simple mechanical system (sequential contractions), acting on a simple reference configuration (nested rings, called a blastula), and deforming into a simple final configuration (nested tubes, called an animal). The same molecular pathways used for force actuation at this early stage will be available for animal motion and muscle contraction later on in development.

[1] In rays, growth of a very wide pectoral flap along the Dorso-Ventral edge is a secondary process during embryogenesis.

[2] The A-P asymmetry in vertebrates stems from a polar distribution of vitellus in the oocyte, further amplified by the mechanism of sperm entry across the oocyte membrane. Here, we shall not discuss further this asymmetry.

We show here that the blastula presents an additional, second-order division in radial sectors. We demonstrate that buckling of the sectors drives the formation of secondary cylinders or tubes that will eventually become the sensory organs.

II. Materials and methods

For embryos until day 3 of development, the preparation of chicken embryos for optical microscopy follows a method described in Ref. 13. Older embryos (days>3), used especially for observation of eye development, are removed from their vitelline membrane, and the head is gently taken out from the amniotic sac by aspiration with a 3ml plastic Pasteur pipette, which is cut at the end to have a diameter slightly greater than the diameter of the embryo body (hence a diameter of the pipette tip in the 1-2 mm range). Embryos can be oriented in different positions for observation by rocking them carefully with tweezers. In our optical microscopy set-up, contrast is enhanced by two-slit illumination working as a Mach-Zender type interferometer [13].

Particle Imaging Velocimetry (PIV) was performed using the ImageJ software developed by Wayne Rasband at National Institute of Health, and the Tracker Plugin for ImageJ developed by Olivier Cardoso and Bérangère Abou (all plugins are freely available upon request).

Elastic modulus measurements were performed by Atomic Force Microscopy (AFM) in force spectroscopy mode. Embryos were extracted from the egg and pinned on rubber, measurements were done in a fluidic cell, in Phosphate Buffer Solution (PBS, Dubbelco). The AFM measurements were performed with a JPK nanowizard 1 AFM (JPK BioAFM Business 12489 Berlin, Germany). The cantilever used had a 2µm round bead, with a spring constant of 0.067N/m (NanoAndMore Spilburg Bld. A1 Steinbühlstrasse 7 D-35578 Wetzlar Germany). The maximum force applied by the cantilever was set as to perform a deformation of approximately 0.5 µm. Young modulus was determined using a simple Hertz model with the JPK data analysis tool.

All animal experiments presented here are authorized by French law R214-87 modified by the Décret n2013-118.

III. Results

A. The blastula presents a second order radial division into sectors

We observed the structure of the early blastula[3] by optical microscopy. The most conspicuous structures are the encased rings already mentioned (Fig. 2A). Radial sectors are also visible (Fig. 2B, C) as from day 1 of embryo development. An anterior sector is located between 10 and 2 o'clock (12 o'clock corresponding to the anterior part of the embryo, Fig. 2B), and two symmetrical sectors located at 2-5 o'clock and 8-11 o'clock (Fig. 2C). For the sake of clarity, we make reference in the figures to Hamilton and Hamburger staging [14]

[3]Called blastodisc in the case of chicken.

(HH stages). We found that the anterior sector presents further subdivisions (Fig. 2B). We present the schematic structure of the blastula in Fig. 2D. The radial boundaries of the sectors cross the orthoradial ring structure (Supplementary Material Fig. 1).

B. The sectors transform into sensory organs

We followed dynamically the subsequent movements of these sectors. We observed that the anterior sector locks the mouth (Fig. 2B, Video 1) and the eye precursors (Fig. 3A, Videos 2-4), while the second sector locks the otic (ear) territory (Fig, 3B, Videos 5-7). Detailed examination reveals that the otic territory represents only an orthoradial slice of the sectors located at 2-5 and 8-11 o'clock (Fig. 3C, see especially the last frame in Video 5, and also Supp. Material Fig. 2). We observed that the eye and the ear form respectively by rapid contractions and invaginations of the discoidal ocular (Fig. 4A, Video 8) respectively otic (Fig. 4B, Video 7, 9) placode.

C. The tissue comprising the sectors is excitable

Returning to much earlier stages of development, and filming with a finer temporal resolution, we observed sporadic twitches (contractions of 15% amplitude) of the embryonic tissue already at the blastula stage, prior to actual morphogenesis, Stage HH5 (Fig. 4C, Video 10, other events available) demonstrating an intrinsic contractility and excitability of the tissue, quite similar to that already observed for amniotic sac contraction [10]. We also found that the tissue responds to electric shocks of 0.5 V by a rapid contraction, as we had found previously (data not shown) [13].

D. Involvement of neural crest cells in eye and ear formation

The movements described above deal with the ectoderm. Ectodermal cells form an epithelial sheet of cells, and they don't migrate individually. We observe in our experiments that epithelial cells in the neural crest undergo a transition to become migrating Neural Crest Cells (NCCs) [15]. While this event is quite well documented, we are able to observe it in sufficient detail to see that NCCs migrate around the eye placode and around the ear placode (Videos 11, 12, see also Videos 7 and 9 Fig. 5A, B). The simplest interpretation is that the close contact between the placode ectoderm and the underneath neural ectoderm hinders cell migration across the placode, and NCCs simply migrate around the obstacle formed by the presumptive eyes and ears. This explains why these areas are softer, eventually, being devoid of the layer of cells which is known to differentiate into cranio-facial bony structures [15]. One important observation is that the onset of NCCs migration away from the median axis correlates with a shortening and widening of the neural tube (Fig. 5C see for example Videos 12 and 13). It makes sense, that, if intercalation of cells is a mechanism for chord or neural tube convergence and extension [16], reciprocally, desintercalation of cells to form migrating cells induces a shortening and widening of the neural tube.

E. Secondary tube formation occurs by buckling along lines of elastic contrast

In our experiment, the peripheral stretch of the embryo is released when we cut the vitelline membrane. The embryo is therefore less stretched radially than physiologically. We observed frequently that the otic territory buckled prematurely, in a hairpin pattern forming a slit-like furrow, instead of buckling in the form of an ear (Fig. 6, Video 14). In Fig. 6 Top, the otic sector is particularly well visible (arrowhead), with the placode territory itself intersecting the sector.

The difference in cell texture suggests a difference in mechanical properties. We performed Atomic Force Microscopy (AFM) measurements on embryos around the otic territory prior to formation of the otic placode (HH 10), and found an elastic contrast, preceding ear formation (Fig. 7A). Visual inspection shows that the embryo is narrower and less dense in the area of the presumptive ear. When the embryo is bent with a motorized glass needle, it flexes in the area of the presumptive ear, confirming that this area is softer (Fig. 7B, Video 15).

F. A sequence of contractions transforms a planar sector into a tubular secondary organ

Both ear and eye territories undergo considerable movements during morphogenesis of the corresponding organs. Eye stalks and cups expand away from the median axis against the ectoderm to complete the eye placode morphogenesis (Fig. 8A) until contraction and invagination occur (Videos 16-18). In the case of the ears, the otic sector undergoes a sequence of dipolar and quadrupolar deformations. First, the sector is driven posteriorly by blastula rotation and gastrulation [8]. Next it is sheared in a hyperbolic pattern by primitive streak recession and chord extension [9]. It is then dragged towards the median axis by a dipolar pull of the neural folds [17]. Once the hairpin is positioned on the dorsal area, the ventral pull of the cardiac ring shears the ear territory anteriorly (Fig. 8A, Videos 19, 20 ; Video 20 shows a profile view of the contraction of the anterior ring, or cardiac crescent, of the blastula, showing the mechanism of head flexure). Finally, the ear territory undergoes a quadrupolar contraction colinear with the DV boundary (Fig. 8C, Videos 20, 21 ; Video 21 shows the movement of quadrupolar contraction in the otic area used to extract the PIV map shown in Fig. 8C). This finishes the closure of the hairpin along the ventral boundary. Eventually, a well characterized ear placode is formed. While these movements may seem very complex, they correspond to a rational sequence of dipolar and quadrupolar contractions following the rings and sectors boundaries.

The main dynamic difference between ear and eye lies in the fact that the eye is formed by a double invagination of the surface epithelium and of the underlying neural epithelium (forming the lens and the eye globe), while in the ear there is a single inwards fold forming the ear pit. This difference can be traced back in Fig. 3 to the fact that the eye territory is one ring more central than the ear territory.

G. Modelisation

We may use a simple model of tissue advection in viscous flows [8], to generate very simply otic placodes from blastodisc sectors (Fig. 9A Video 22). We start from a trapezoidal line representing the contour of one sector, intersected by one ring. The speed **V** of the tissue is given *via* the stream function formalism by :

$$\mathbf{V}=\mathbf{curl}(\mathbf{A}) \qquad \text{Equ. 1}$$

with $\mathbf{A}(x,y,z)=(0,0,\Psi(x,y))$ and with $\Psi(x,y)$ the stream function, given explicitely by 4 logarithmic vortices revolving around a hyperbolic point. This situation is what is obtained for cells pulling along the DV boundary. The DV boundary is set at y=0, and the pull is exerted by two antagonist lines of cells located at x=a and x=c, with a pull exerted by cells in the segment along [-b,b] in Oy, pulling with opposite signs along Ox, this gives :

$$\Psi(x,y)=\alpha\ln((x-a)^2+(y-b)^2) - \alpha\ln((x-a)^2+(y+b)^2) - \beta\ln((x-c)^2+(y-b)^2) + \beta\ln((x-c)^2+(y+b)^2) \qquad \text{Equ. 2}$$

Typical boundary movements are shown in Fig. 9A, calculated iteratively with a tabler. Moreover, by using unequal values of α and β we can introduce an AP asymmetry. This is expected because the heart induces an asymmetry of the pull. While a difference in magnitude of the force creates directly an asymmetry of the movements, the asymmetry may also come from differences in visco-elastic parameters. Such asymmetries generate anything between a round placode and realistic ear-like shapes (Fig. 9B Video 23). The purpose of this calculation is to show that a very simple quadrupolar dynamics acting on deformable territories is able to generate placodes and ear-like shapes. Since embryo morphogenesis is driven by contractions, it is not surprising that quadrupolar deformations dominate the morphogenetic process. The model predicts qualitatively that animals undergoing a more pronounced head flexure, will have more choncoidal ears *in lieu* of round orifices, as observed.

IV Conclusion

In conclusion, we have shown that, during chicken development, the transformation of a blastodisc into a 3D rudimentary animal follows a deterministic pattern which is present

in the chicken as early as the first day after the egg is laid. The partition into rings and sectors leads to a structure with main tubes in the AP direction and secondary tubes in the perpendicular direction. The mechanism of formation of both tubes is similar (Fig. 9D). The presumptive organ domains are not standing waves of chemicals *à la* Turing [18], but an elastic texture with straight boundaries that deform dynamically. Since the secondary tubes are initially locked to radial sectors, they form at right angles to the main AP tubes. Since these tubes form as a secondary process, they are smaller, and since they form on the dorsal side of the already formed neural tube, they naturally form sensory organs.

We have observed in the experiments that if buckling occurs prematurely, the fold follows the edges of the sector and takes on a hairpin slit form, instead of forming a cylindrical tube. This gives a physical explanation to the transition between orifice-like tubes, and gill-like slits : the buckling pattern either follows the edges of the sector, and makes a slit, or rounds off inside a trapezoidal orthoradial section of a sector, and hence pinches off an orifice. Heart shear and head flexure contribute to the formation of an asymmetrical ear by a quadrupolar contraction along the DV boundary, with a singular pinching of the hairpin (See Fig. 9A); this gives an explanation to the morphological difference between mere round orifices, and more convoluted ear forms. This might also give a basis to the physical separation of ears and jaws during evolution [19].

While we have not access to chicken embryos earlier than day 1, existing in vivo images of blastulas of eggs retrieved from hen oviducts prior to shell formation [20, 21] shows a clear pattern of cell texture in rings and sectors (Fig. 10A). Especially, the formation of sectors with smaller cells in a hairpin pattern (cells are smaller in the centripetal direction following the sectors more towards the center of the blastodisc) finds a straightforward explanation when remembering the dynamics of the first cell divisions. Indeed, it is known that, in vertebrates, the first two cell divisions occur in the average blastodisc plane and generate a planar pattern of four cells. The next division is radial (Fig. 10B Right, top-left). The next cell division is perpendicular to the blastodisc plane and it generates the underneath layer [22]. The next rounds of divisions occurs in the concavities (hairpins) of the third divisions, towards the center of the blastodisc (Fig. 10B). The greater size of the peripheral cells is ascribed classically to yolk inhibition [23]. Errera's rule [24] or physical stress equilibrium [25] both lead to a minimal (minimal elastic energy, or minimal wall area) radial and orthoradial partition of sectors during cleavage, generating a structure in

concentric rings, with criss-cross sectors forming hairpins (and these are also found in soap bubbles arrangements [24]). In conclusion, the basic form of vertebrates, which consists of elongated nested tubes, decorated by perpendicular orifices diving down into the brain is a physical attractor of minimal cleavage, followed by deterministic buckling along the biaxial principle lines of the cleavage. The main feature of this process is the topological conservation of radial and orthoradial planar boundaries, which project themselves onto axial Antero-Posterior and orthogonal Medio-Lateral 3D tubes, giving support to the existence of a vertebrate structural archetype. The conservation of the texture during the entire morphogenetic process is possibly related to the locking of cell division dynamics onto the already existing pattern of extracellular matrix at the moment of division, as reported in cell biology studies [26], and to the very slow creeping fluid dynamics [8].

Acnowledgement

We thank Nicolas Chevalier for his interest and support, and for a careful reading of the manuscript.

References

1. K. E. von Baer, *Über Entwickelungsgeschichte der Thiere* (Ludwig Stieda , Königsberg 1828).

2. W. His, *Unsere Körperform und das physiologische Problem ihrer Entstehung. Briefe an einen befreundeten Naturforscher* (Engelmann, Leipzig 1874).

3. C. V. H. Baker, M. Bronner-Fraser, Dev. Biol. **232**, 1–61 (2001).

4. V. Fleury, Chaos, Solitons and Fractals, **105**, 230-234, (2017).

5. V. Fleury, N. Chevalier, F. Furfaro, J.-L. Duband, Eu. Phys. J. E **38**, (6), 1-19 (2015).

6. G. W. Brodland, D. I.-L. Chen, J. H. Veldhuis, Int. J. Plastic. **22**, 965 (2006).

7. D. A. Voronov and L. A. Taber, Dev. Dyn. **224**, 413 (2002).

8. V. Fleury, Organogenesis, **2**, 1 6-16 (2005).

9. V. Fleury, Biosystems, Special issue “Morphogenesis”, **109**, 460-474 (2012).

10. V. Fleury, A. V. Murukutla, A., N. Chevalier, B. Gallois, B., M. Capellazzi-Resta, P. Picquet, A. Peaucelle, Phys. Rev. E **94**, 022426-022444 (2016).

11. G. Shah, K. Thierbach, B. Schmid et al., Nature Comm. **10,** 5753 (2019).

12. N. Tipping and D. Wilson, Anat. Rec. (Hoboken) **294**, 1143 (2011).

13. V. Fleury, A. V. Murukutla, Eu. Phys. J. E. **42**, 104 (2019) doi:10.1140/epje/i2019-11869-8.

14. V. Hamburger, H. L. Hamilton, Journal of Morphology **88** (1), 49–92 (1951).

15. H. Etchevers, E. Dupin, N. Le Douarin, Development **146**: dev169821 (2019).

16. R. Keller, *Science,* **298**, (5600), 1950-1954 (2002). DOI: 10.1126/science.1079478.

17. V. Fleury, Eu. Phys. J. App. Phys. **45**, 30101 (2009).

18. A. M. Turing, Phil. Trans. Roy. Soc. London B **237** (641), 37-72 (1952).

19. F. Mao, Y. Hu, C. Li, Wang, M. H. A. Chase, A. K Smith, J. Meng, *Science* **367** (6475) 305-308 (2020).

20. H. Nagai, M. Sezaki, K. Kakiguchi, Y. Nakaya, H. Ch. Lee, R. Ladher, T. Sasanami, J. Y. Han, S. Yonemura, G. Sheng, Development 142, 1279-1286 (2015).

21. H. C. Lee, H. J. Choi, T. S. Park, S. I. Lee, Y. M. Kim, S. Rengaraj, H. Nagai, G. Sheng, J. M. Lim, J. Y. Han, PLoS ONE **8** (11), e80631, (2016).

22. G. Forgács, S. A. Newman, *Biological physics of the developing embryo,* (Cambridge University Press 2005).

23. E. B. Wilson, *The Cell and development in heredity*, Third edition (Macmillan, New York, 1928).

24. S. Besson and J. Dumais, Proc. Nat. Acad. Sci., **108** (15), 6294–6299 (2011).

25. M. Louveaux, J. D. Julien, V. Mirabe, A. Boudaoud, O. Hamant, Proc. Nat. Acad. Sci., **26**, 113 (30), E4294-303 (2016).

26. M. Théry, V. Racine, A. Pépin, M. Piel, Y. Chen and M. Bornens, Nat. Cell. Biol. **7** (10), 947-53 (2005).

Figures and Figure Captions

Figure 1

Figure 1 Four animals, from ancestral lampreys to sharks, stingrays and birds. The ancestral archetype is that of a tubular animal (Top-Left, the lamprey), with orifices located perpendicularly to the main axis ; we count the eyes as such orifices; the mouth is a special case in that it is colinear with the tubes axis due to its position at one end. In fish, the lateral orifices may be instead slits, as in sharks (Top-Right), or organs in between slits and orifices, as in stingrays (Bottom-Left). Please note that the orifices on the sides of the stingray mouth are the ears. Stingrays have their eyes on the dorsal side, their ventral sensory organs help them capture and eat preys they can't see. In amniotes (Bottom Right), there is an additional head flexure, and the ear orifice is pinched at its Dorso-Ventral boundary, with a slit-like feature detached from the ear and contributing to jaw and gum formation. (Photo Lamprey

: Blinkwinkel/Alamy, Stingray : Jorge Felix Costa, Vulture Dan Russel, Shark : Saberrex Strongheart).

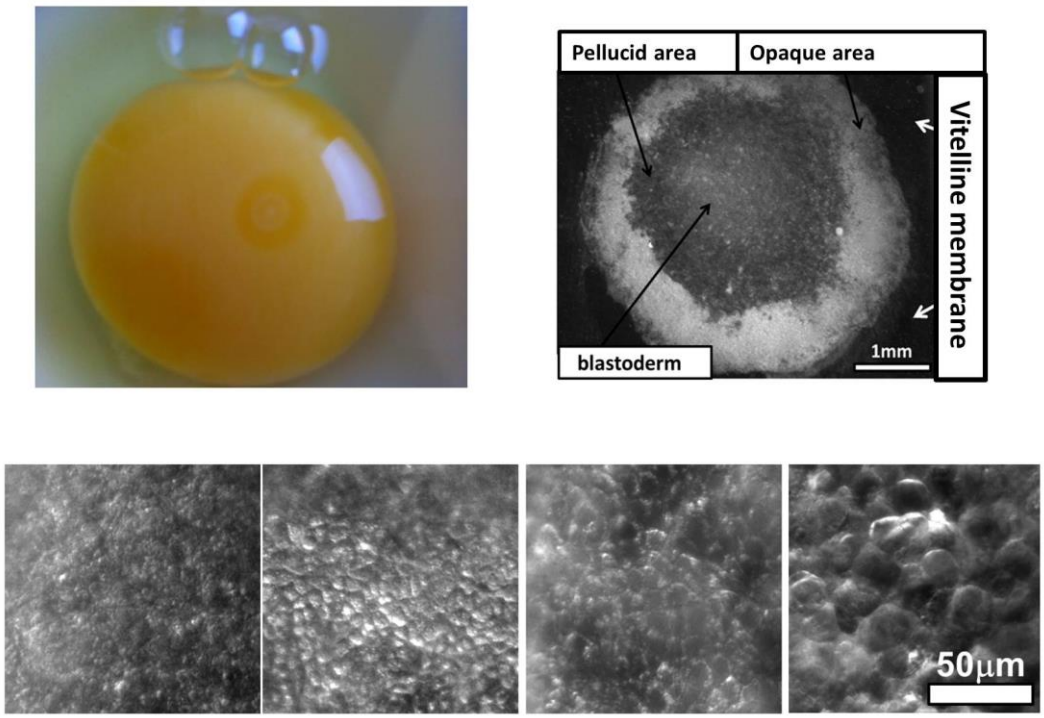

Figure 2A

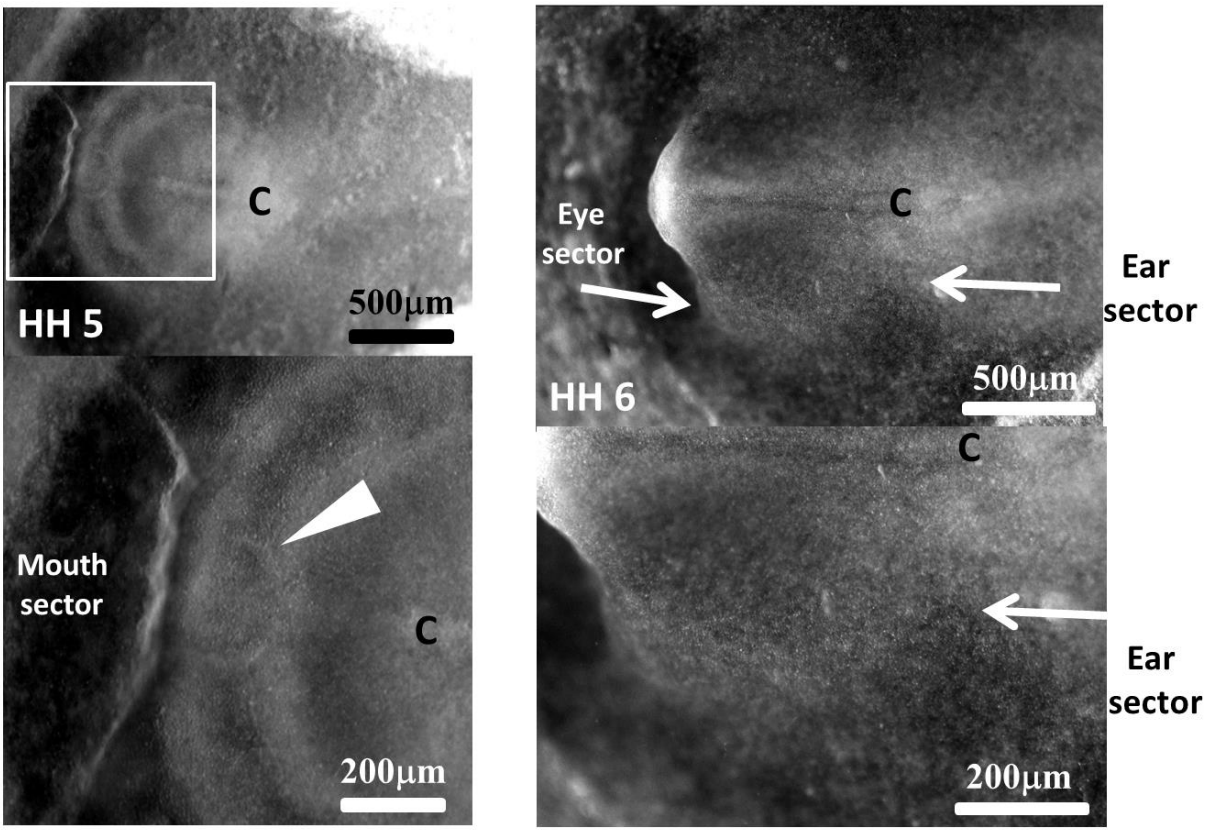
C
HH 5
500μm
Mouth
sector
C
200μm
Eye
sector
C
Ear
sector
HH 6
500μm
C
Ear
sector
200μm

Figure 2B

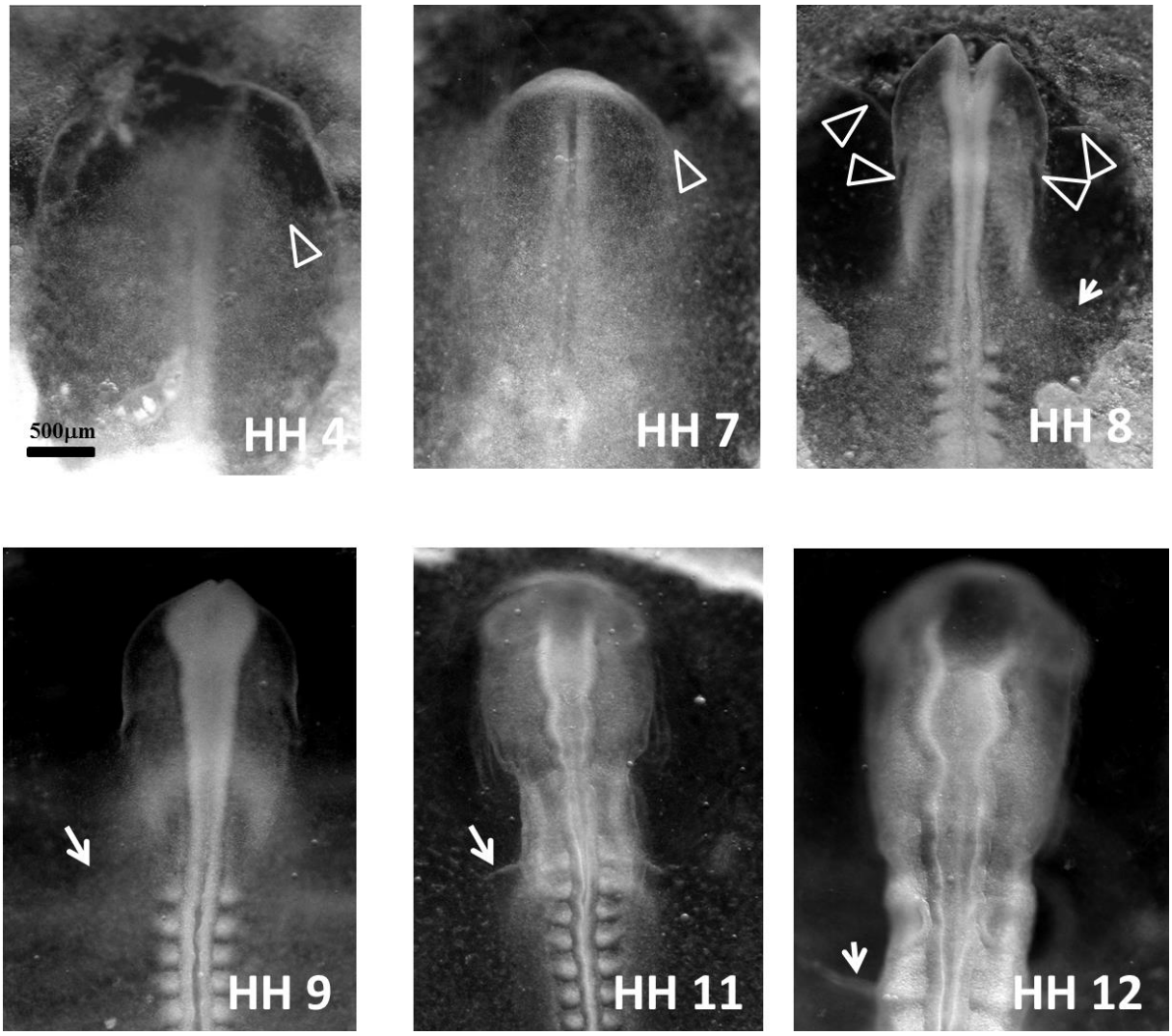

Figure 2C

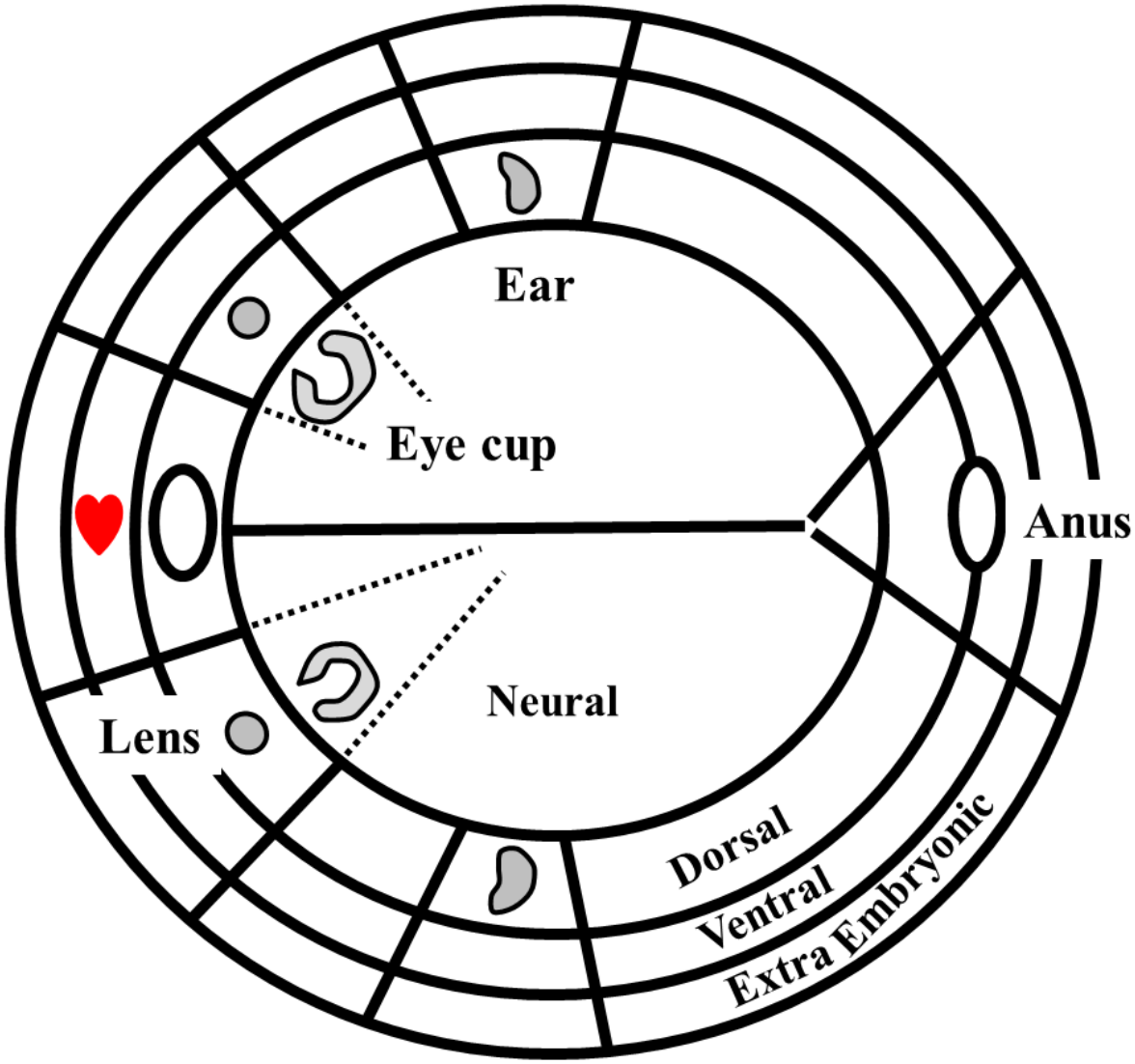

Figure 2D

Figure 2 Fig. 2A (Reprinted from Ref. 5). Optical microscopy of carefully rinsed blastulas (HH 1) show a textural pattern in rings, corresponding to the presumptive territories of the different body compartments. The rings are associated to different cell sizes, central cells being larger than peripheral cells. Fig. 2B In the next hours, a secondary structure in sectors becomes clearly visible (at earlier stages gastrulation movements render images more noisy). One anterior sector will correspond to the mouth territory (Fig. 2B Left). The arrowhead points to the stomodeum (mouth precursor, arrowhead in Fig. 2B), forming in front of the chord (C) and locked by the most anterior sector. Fig. 2B Right : One next sector corresponds to the presumptive eye territory and the next sector corresponds to the ear

territory (arrows). Fig. 2C, during the second and third day of development, the territories deform and the relationship between parts becomes more remote, but the boundaries become actually more visible. The eyes correspond to the apex of the anterior sector (arrowheads), and the ears correspond to the apex of the second sector. The continuity between the boundaries of the extraembryonic territories and the boundary of the ear itself is visible in the bottom-right image (arrows). Fig. 2D Scheme of the blastula prepattern. There exists a structure in rings corresponding in centrifugal order to neural territory, dorsal territory, ventral territory, and extra-embryonic organs. These rings are intersected by a structure in sectors. Trapezoidal territories limited by intersection of rings and sectors correspond to presumptive mouth, eyes (lens and eye ball) and ears territories which round off during morphogenesis (the nasal area was not investigated in this study). One sector also corresponds to the cardiac territory.

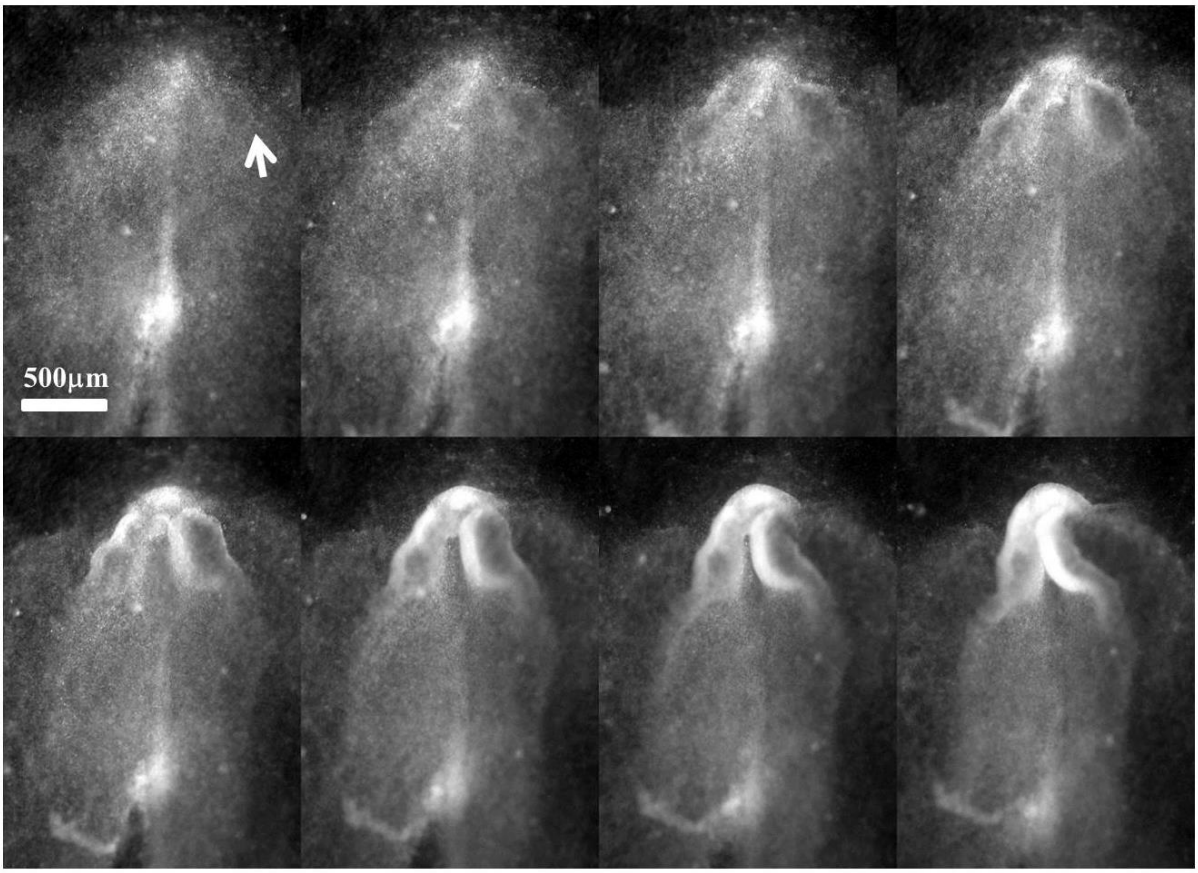

Figure 3A (Top)

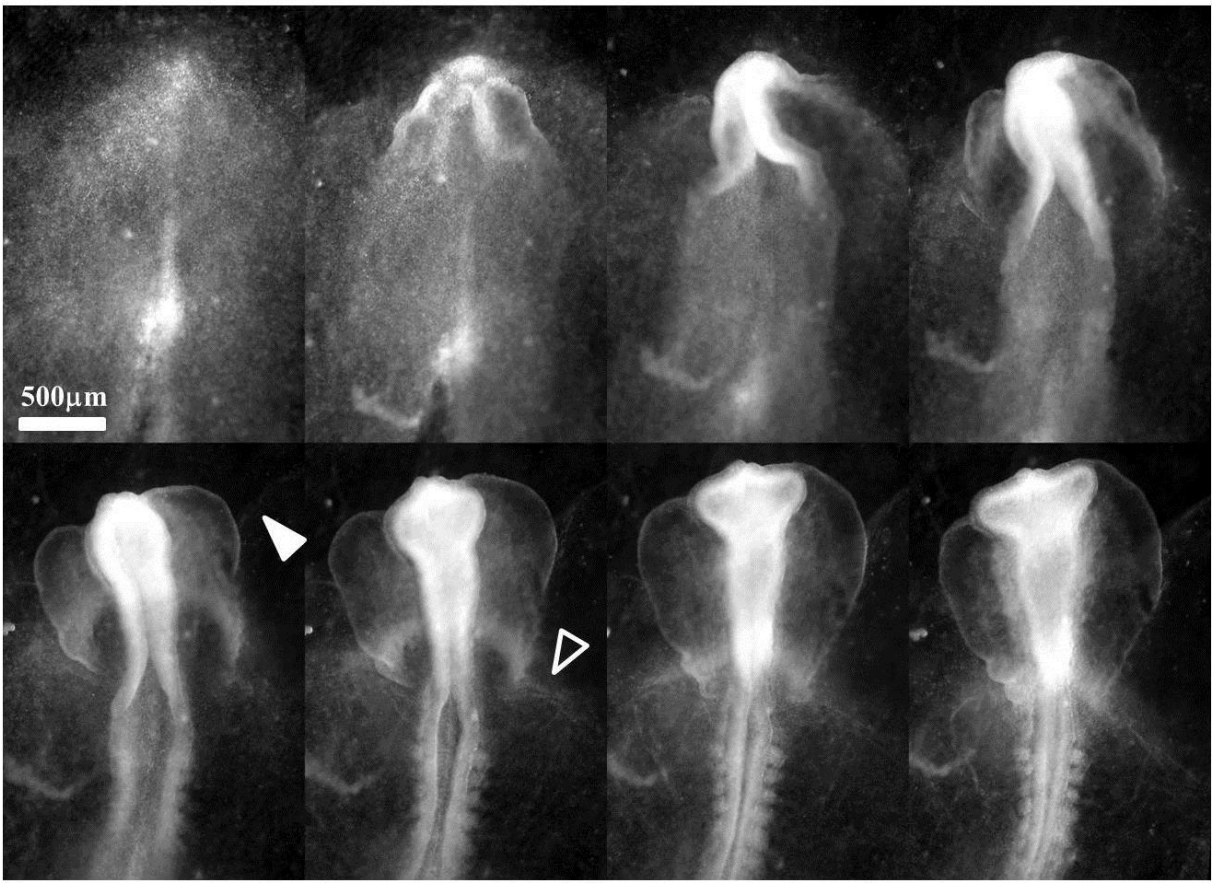

Figure 3A (Bottom)

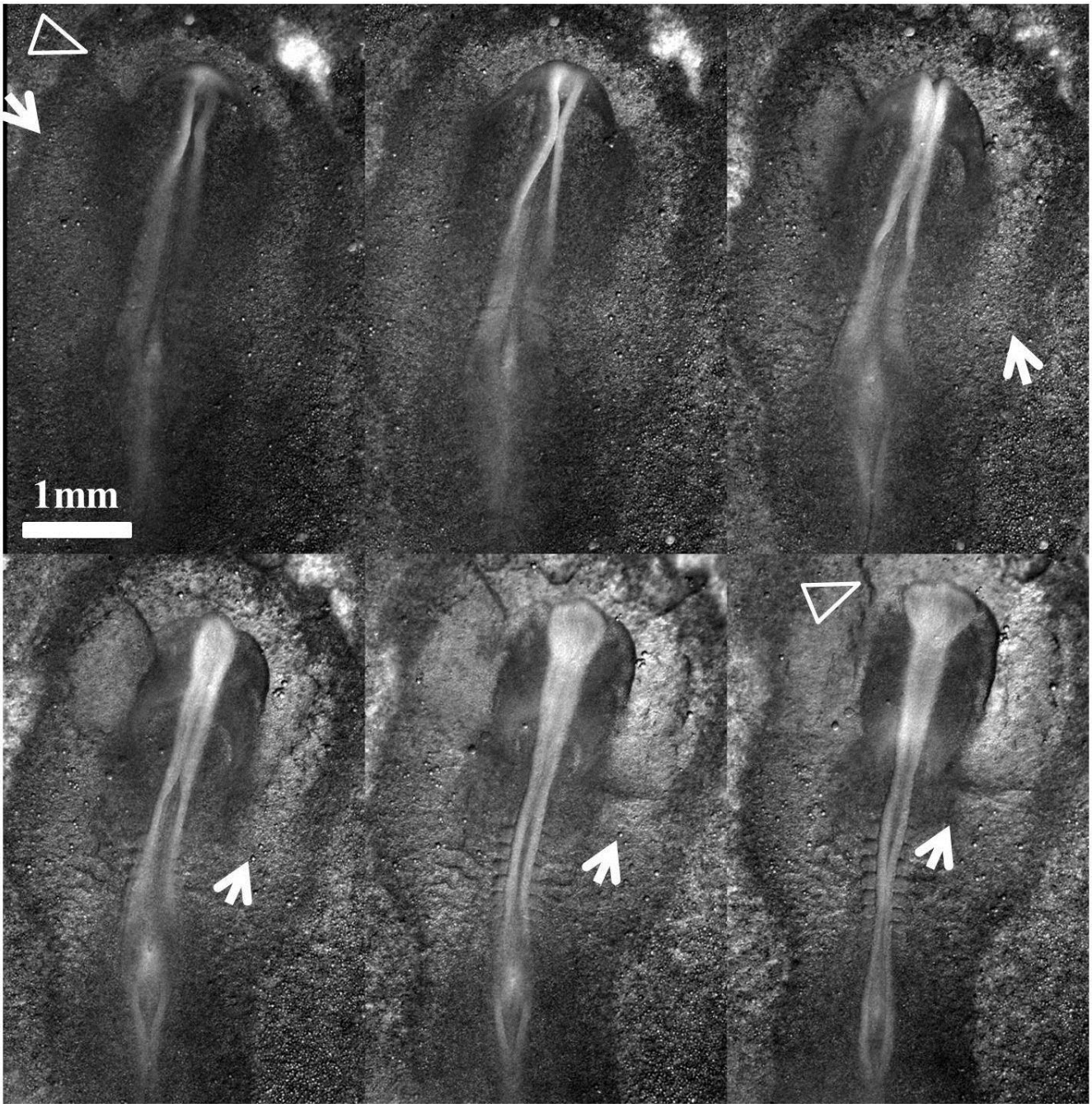

Figure 3B (Top)

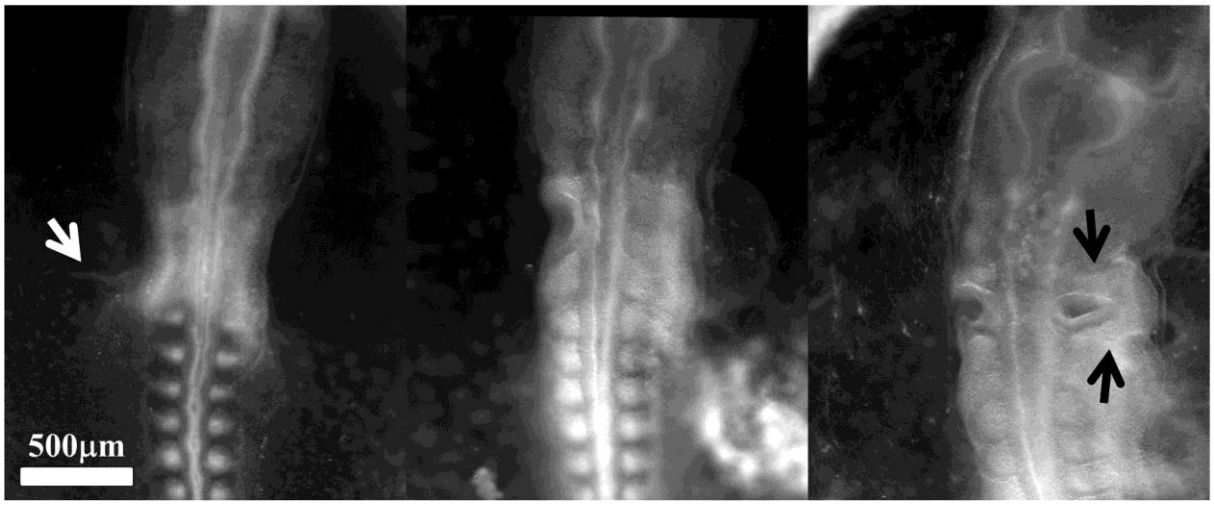

Figure 3B (Bottom)

Figure 3 Fig. 3A.The top mosaic shows the early stages of Time-Lapse in Video 5 (HH5); the second mosaic shows the entire Time-Lapse (HH stages from 5 to 10) up to expansion of the eye stalk (eye stalk expansion is discussed in Ref. 16). The video shows that the presumptive eye territory is exactly the corner in the anterior sector of the blastula sector (arrow). This is also quite visible in Videos 2 and 3. The boundary of this sector remains visible in the embryo as a thin membranous ectodermal flap homolog to the cheek wrinkle. The sector continues away towards the extra-embryonic organs where it localizes the thinner part of the pellucid area, where the boundary of the sector remains visible (arrowhead). Fig. 3B The next sector localizes the ears. The top mosaic shows the T-L (from Video 5) of the transition from a roughly horizontal blastula to the roll up of the embryo body (HH stages from 6 to 8). Again we observe sharp boundaries in the entire blastula, the anterior sector (arrowhead) corresponds to the already evoked ocular sector, while a second sector (arrows) is advected towards the neck and corresponds to the presumptive otic territory. The sectors span the entire blastula and are visible in the extraembryonic territory where they form larger portions. The bottom images (from Video 6) show three snapshots (same embryo) of ear formation at the apex of the sector which now finds itself advected on top of the neural tube (HH stages from 10 to 13). The black arrows in the last image point to the edges of the hairpin in which the otic pit has buckled downwards towards the neural tube. Please note that there is a reproducible temporal delay between left and right ear formation. Buckling

proceeds more rapidly on the right side (to the left in Fig. 3B Bottom Right, since the embryo lies ventrally and is observed dorsally).

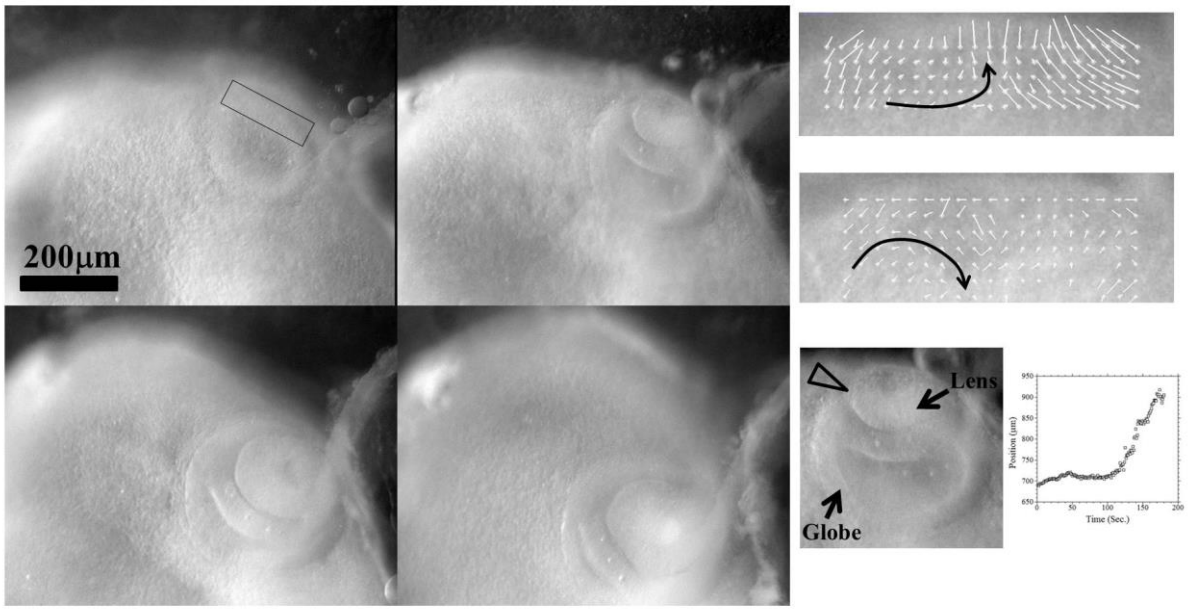

Figure 4A

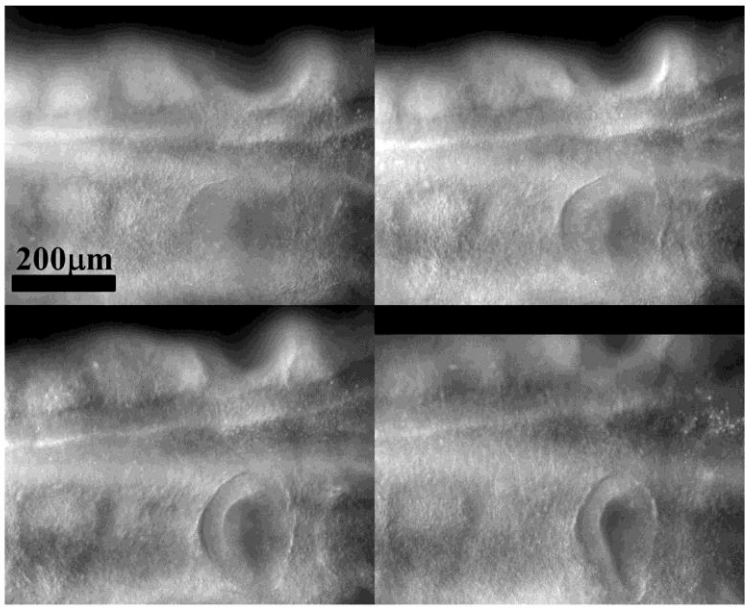

Figure 4B

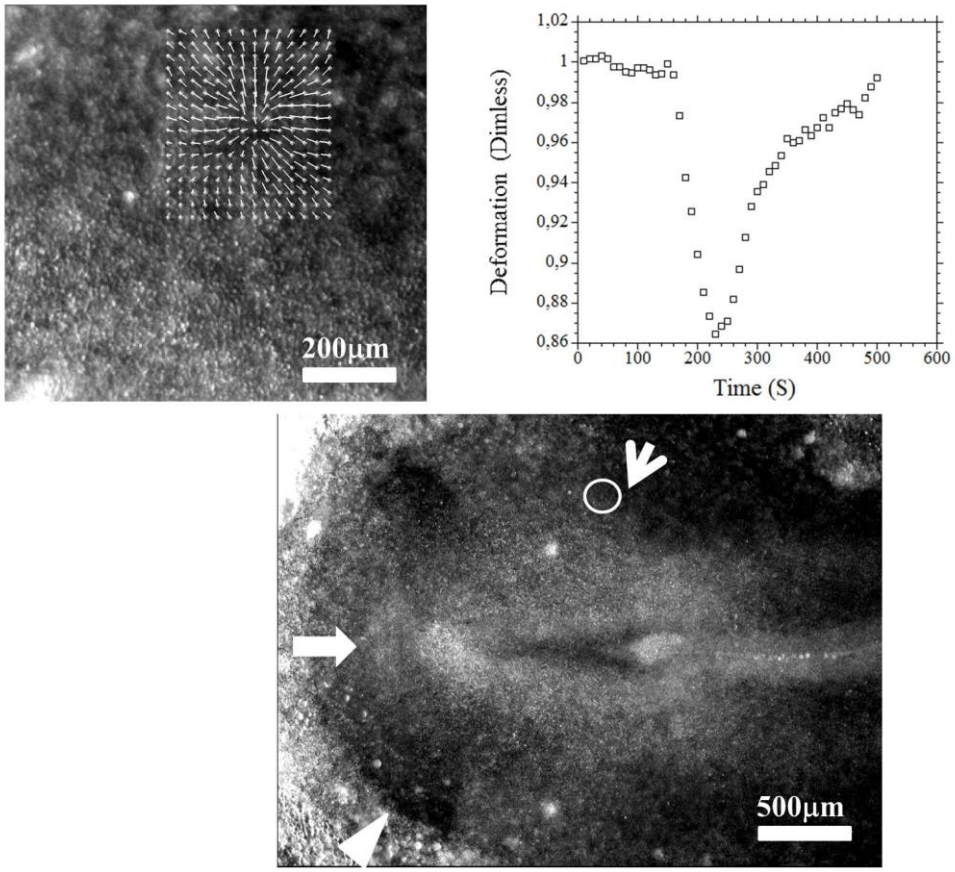

Figure 4C

Figure 4 Fig. 4A In vivo observation of eye formation shows a sudden superficial contraction generating the eye lens inside an eye cup (from Video 8). The four images to the left show a Time-Lapse video of the phenomenon during 6 hours (Mag. 10X). The two PIV analyses show, first (Top), the contracting ectoderm at an early stage when the contraction of the placode generates a constriction in the orthoradial direction and a thickening in the radial direction (the movement points outwards because of constriction). The second PIV analysis shows the subsequent invagination after delamination of the lens ectoderm (the movement points inwards the eye ball because of buckling). The PIV analyses are made at moments corresponding to the Top-Left and Top-Right snapshots. The principle is similar to body formation, except that instead of forming tubes inside tubes, the eye forms a sphere (the lens) inside a sphere (the eye globe). In Fig. 4A Bottom-Right, we show the lens and the globe during formation. The arrowhead points to the line of delamination of the superficial ectoderm which rounds off to form the lens, while the underneath ectoderm invaginates to form the eye globe and retina. The graph in Fig. 4A Bottom-Right, shows the non-linearity of

the temporal evolution of the ectoderm which invaginates (the data points obtained by PIV tracking follow the downwards movement of the invaginating ectoderm). Fig. 4B In the ear, it is observed that the contraction exhibits an asymmetry along the DV boundary, which gives to the ear its specific conchoidal form (from Video 6, see also Video 7 for another example). Fig. 4C When the tissue movements are followed with a fine temporal resolution (1 frame/10Sec.), it is seen that there exist, since the blastula stage, sporadic contractions having a coherent spatial and temporal pattern. The PIV analysis (Fig. 4C Top-Left) and the temporal variation (Fig. 4C Top-Right) are extracted from Video 10. They show a 15% deformation over a 5 Min. contraction. These results show that there exists an intrinsic contractility of the tissue much earlier than the actual morphogenetic events. Also, the textural geometry governs the spatial pattern of forces, and locks the buckling pattern. Bottom of Fig. 4C shows the blastula at the time of this twitch (same embryo). The sectors are visible without any staining. Arrowhead points to the eye sector, the bigger arrow points to the mouth sector, and the smaller arrow to the ear sector.

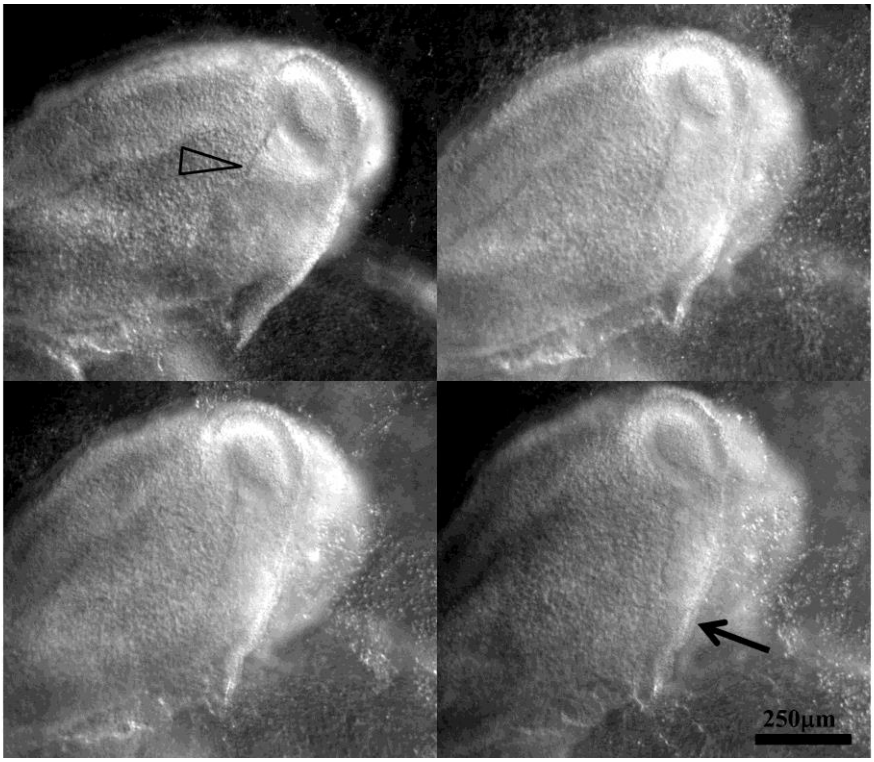

Figure 5A

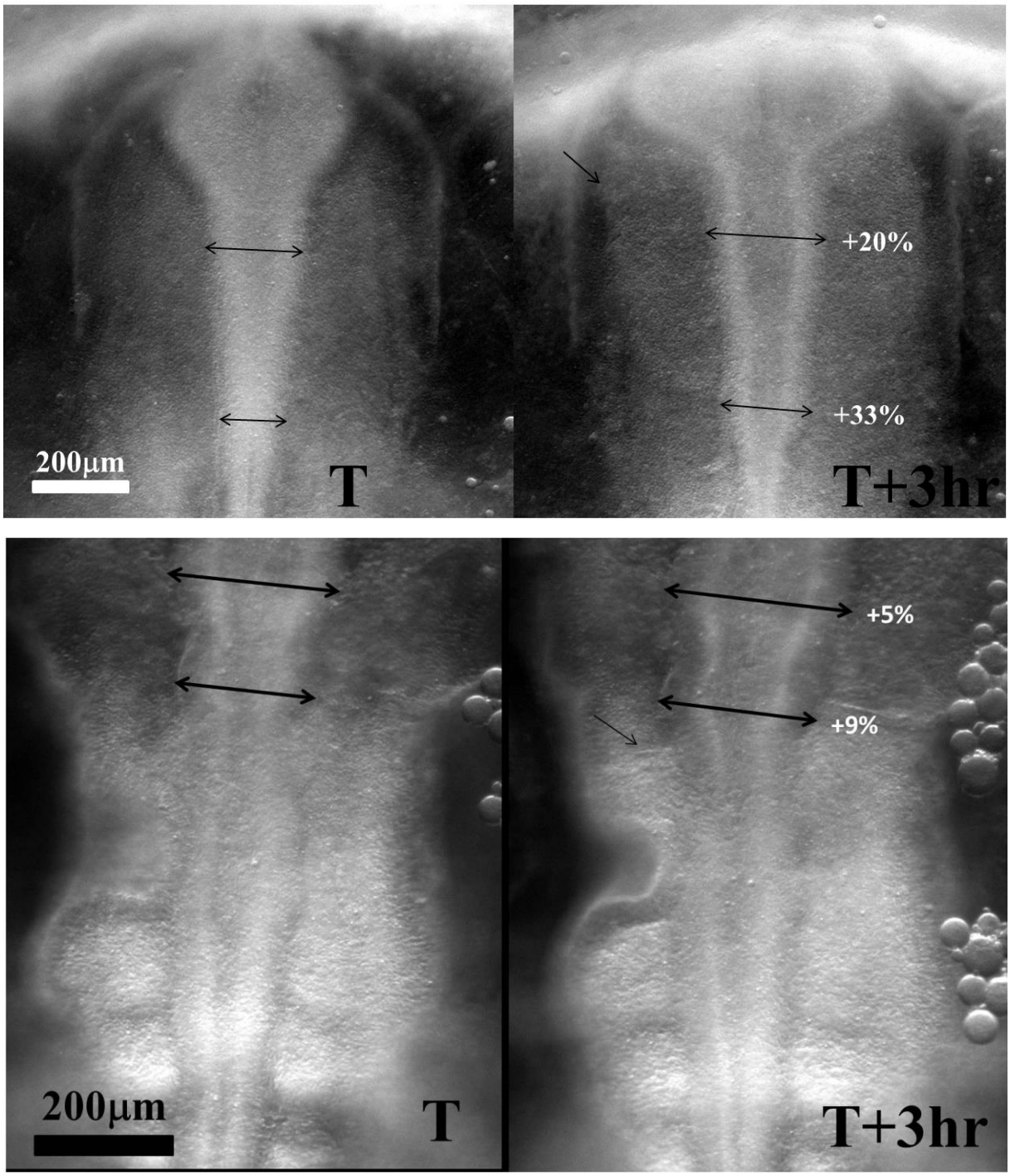

Figure 5B

Figure 5 Observation of the Neural Crest Cells (NCCs). During the morphogenetic movements, NCCs migrate to form bony structures and nerves. We observe quite clearly that the NCCs migrate and swerve around the ocular (Fig. 5A, from Video 11) and otic (Fig. 5B Top, from Video 13) placodes. In Fig. 5A, the straight line emanating from the eye cup (arrow) is actually the very boundary of the eye sector, which forms a wrinkle homolog to the cheek wrinkle on human faces. The continuity between the eye contour and the sector

edge is obvious. The migration of NCCs around the placode explains why eye and ear tissue are softer and prone to generating orifices, surrounded by a thicker protective tissue such as brow bones. Fig. 5B shows that the onset of NCCs migration is associated to a shortening and a widening of the neural tube, which finds a simple explanation in the fact that reduction of the number of cells along the neural tube implies a mechanical shortening by conservation (this is symmetrical to elongation when cells intercalate [16]). The top montage shows the onset and propagation of the cranial NCCs (the thin arrow points to the flow of NCCs, from Video 13). The bottom montage shows the onset and flow of otic NCCs, the thin arrow points to the NCCs flux which is directly visible without any staining.

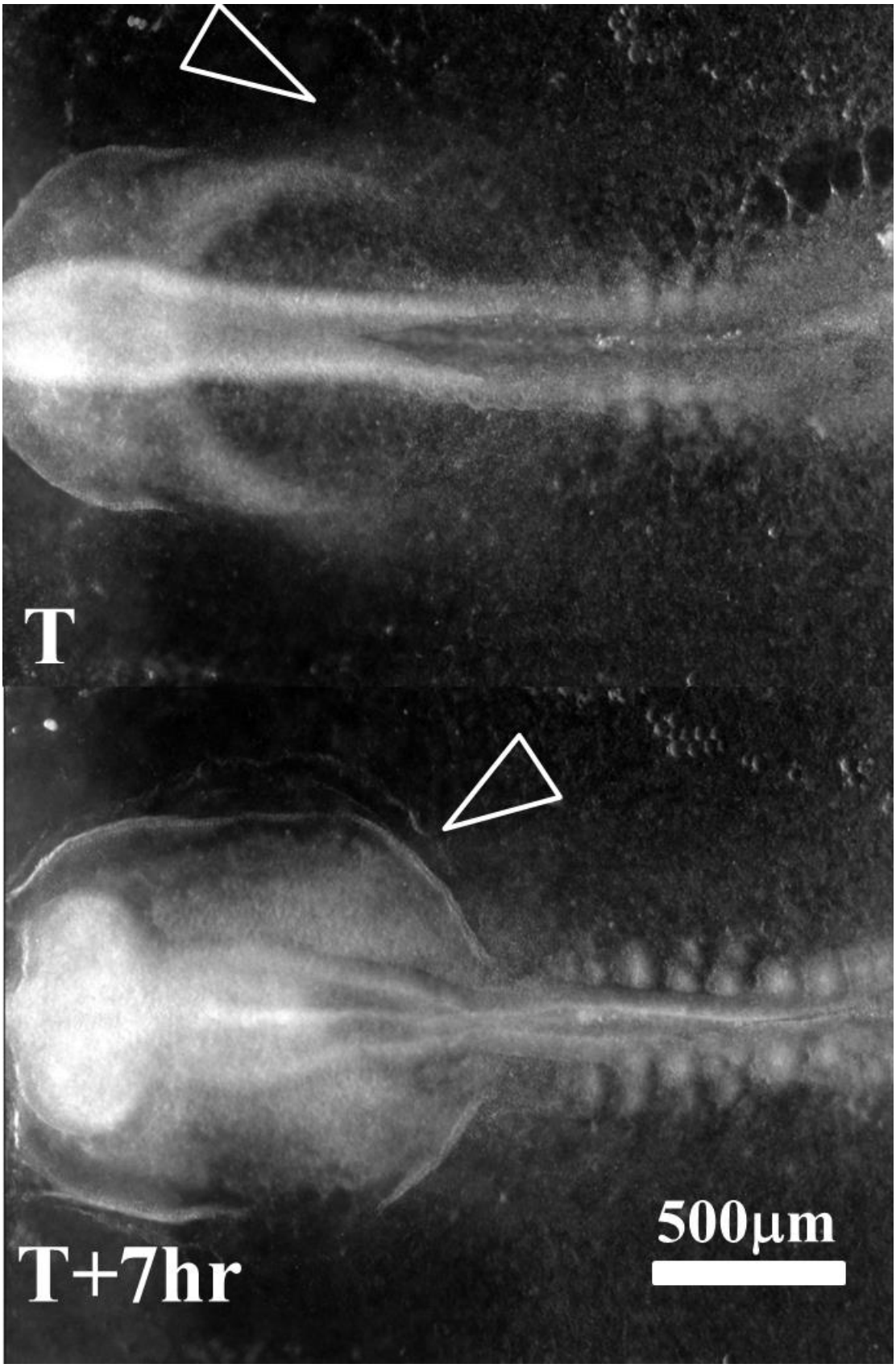

Figure 6

Figure 6 When preparing embryos for optical microscopy, we have to cut them off the vitelline membrane. This reduces the peripheral tension around the embryo. We often observe a premature buckling of the ear sector (arrowhead), in the form of a hairpin instead of an orifice (from Video 14).

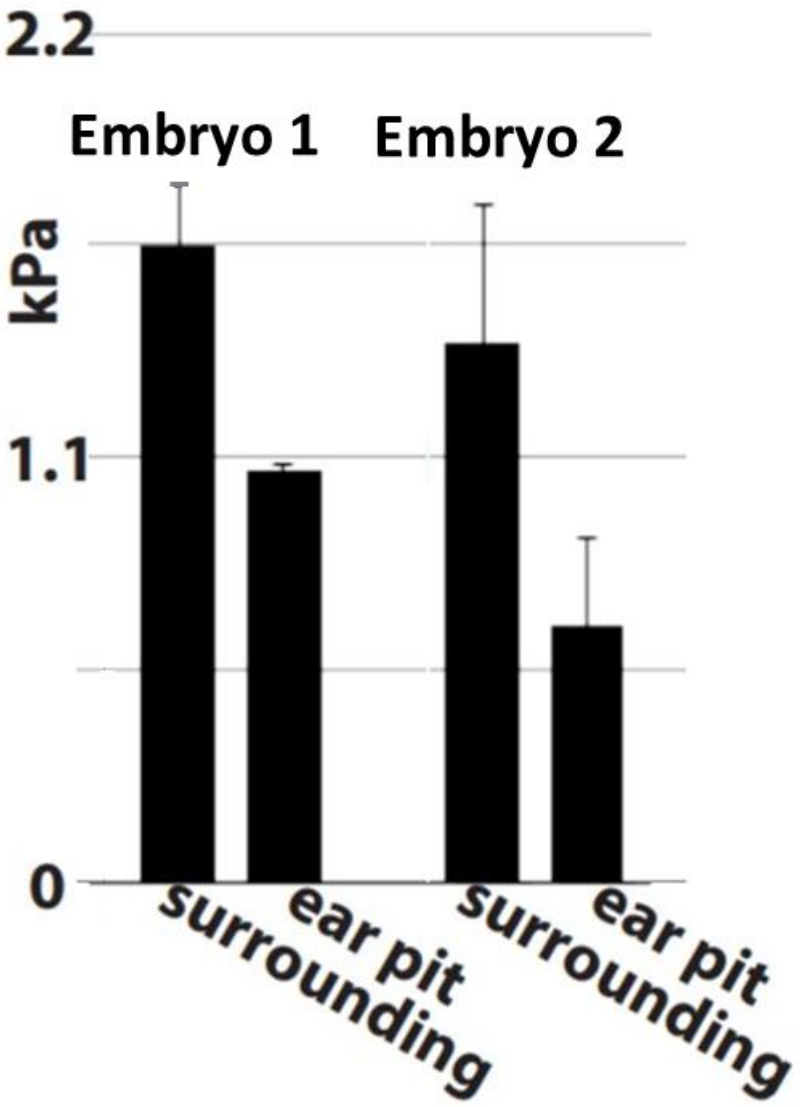

Figure 7A

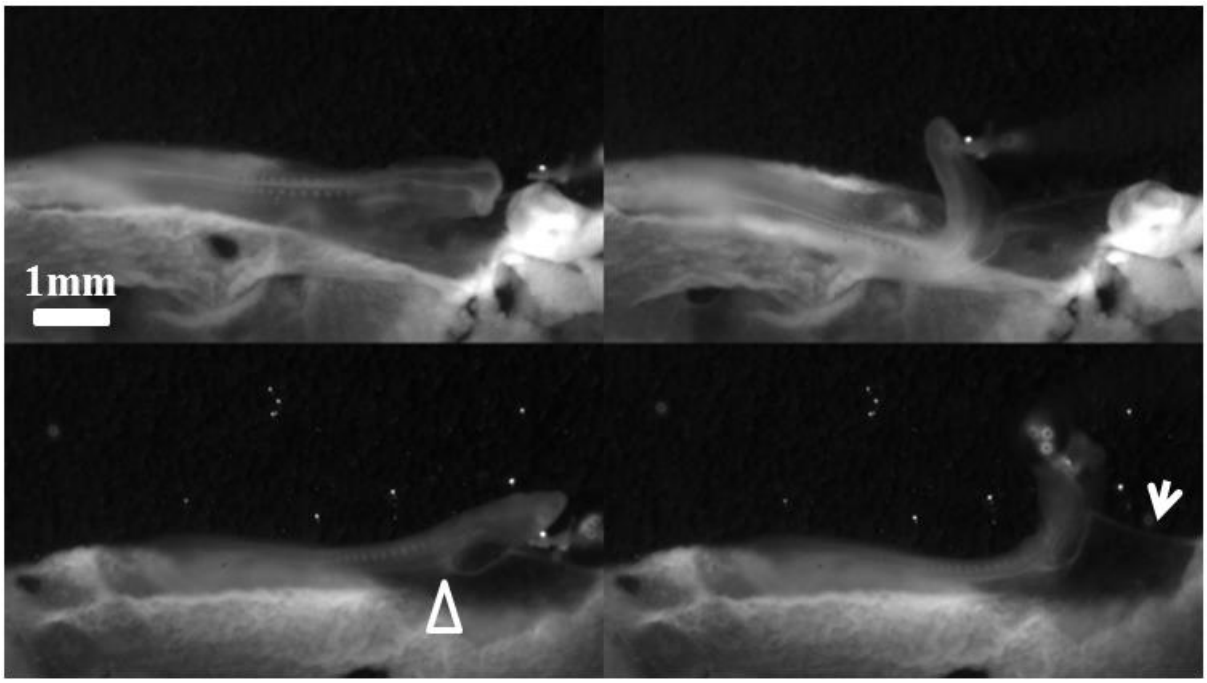

Figure 7B

Figure 7 Fig. 7A We assessed the elasticity of the tissue by AFM. Measurements at HH stage 9-10 (prior to actual ear pit formation). AFM measurements in force spectrosopy mode reveal a softer tissue in the presumptive ear pit, as compared to the tissue around the future ear pit. The elasticy difference just prior to ear pit formation shows an elastic modulus ~0.75kPa in the presumptive ear pit, as compared to ~1.5kPa in the surrounding tissue. Fig. 7B We also flexed embryos at stages HH 10 and 11 in Fig. 7A, with motorized glass pipettes. We observe that when a force is applied perpendicularly to the embryo AP axis, the embryo flexes in the presumptive ear area (and even buckles inwards in this area), confirming that this area is softer.

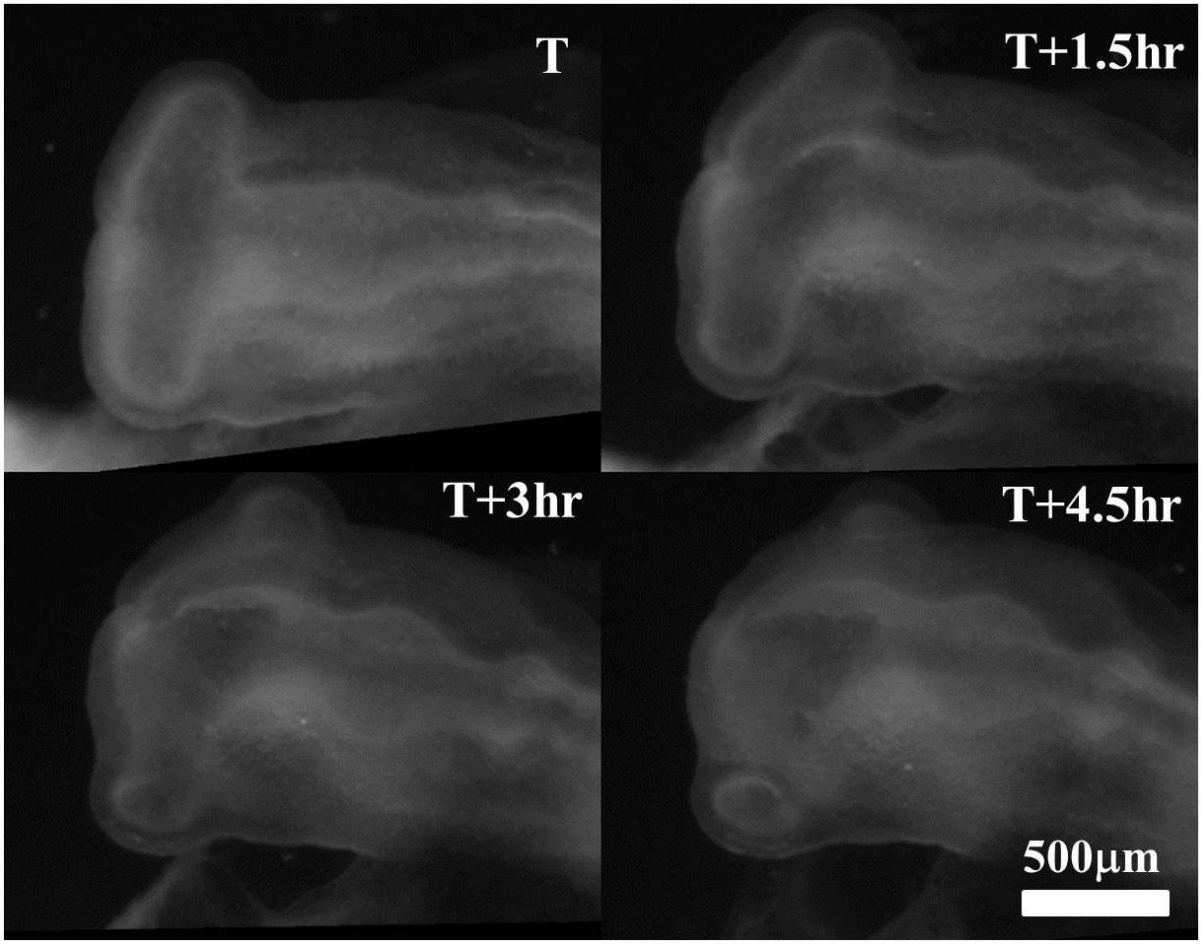

Figure 8A

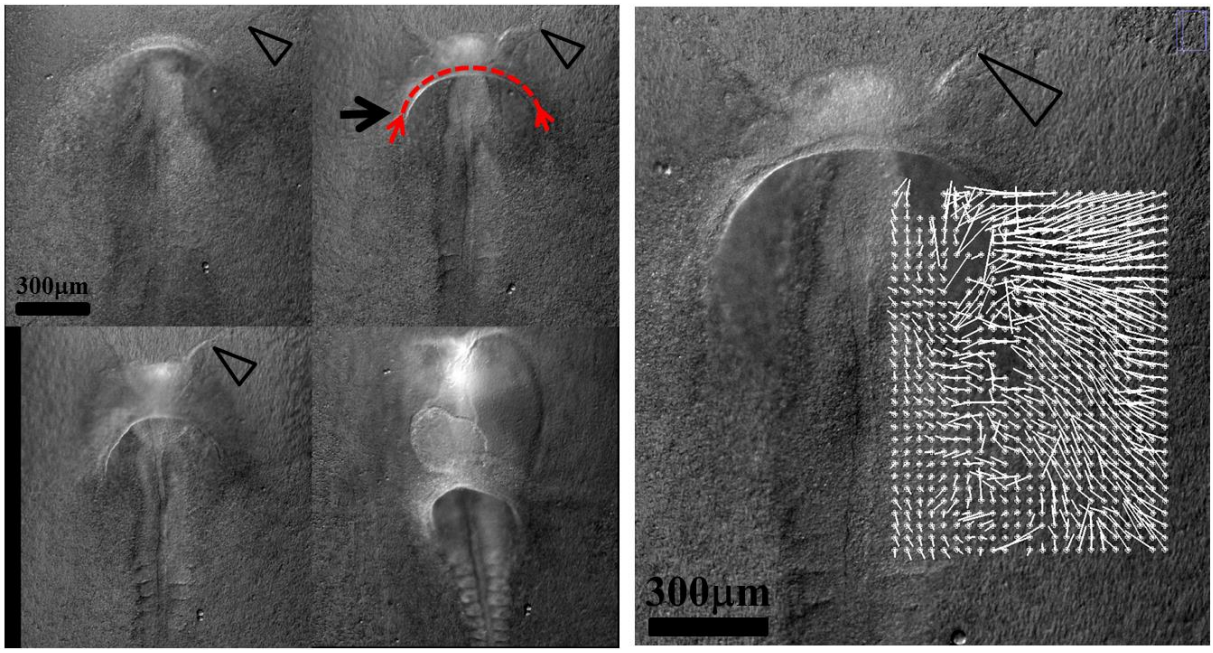

Figure 8B

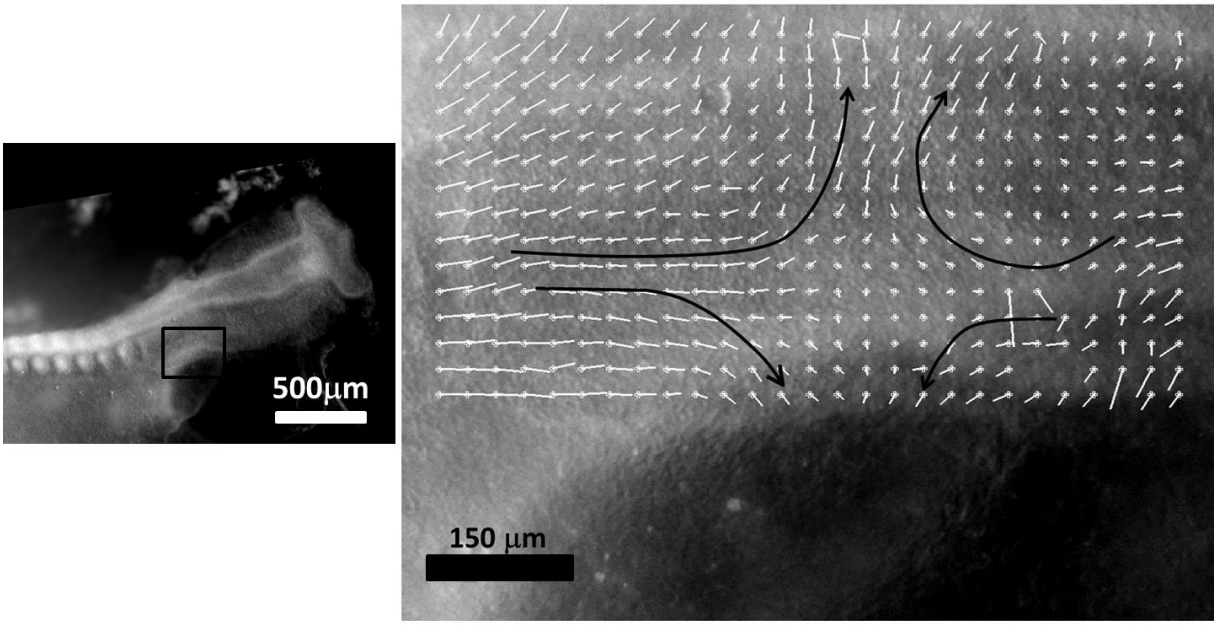

Figure 8C

Figure 8 Morphogenesis of eyes and ears implies considerable movements. Eye movement is simpler to understand, the eye stalk extending in a hammer shape locked onto the eye sector and the eye cup colliding against the ectoderm where the placode rounds off under compression (Fig. 8A, from Video 15). Ear movements are more difficult to understand because there is shear. In addition to the movements described in the literature [7, 9, 16], there exists an underneath dipolar pull by the heart crescent (Fig. 8B), and a quadrupolar winding of the ear territory due to contraction along the DV boundary (Fig. 8C). Fig. 8B Shows four snapshots on the ventral side of the embryo, during establishment of the ear territory. When filmed from underneath, the Time-Lapse microscopy reveals a very important shear of the body tissue by the heart and gut crescent (Arrow), the force is oriented along the purse string formed by the edge (dots). Arrowheads point to the quite visible boundary of the ocular sector. During this shear the tissue is dragged towards the cardiac crescent, and the mesodermal cells are sipped into the cardiac area. Fig. 8C shows the PIV analysis of the contraction during 10 minutes of movement, in the area of the ear territory of a day 2 embryo, HH stage 11 (vectors rescaled to visible sizes). It shows a quadrupolar contraction winding the ear territory towards the dorsal area.

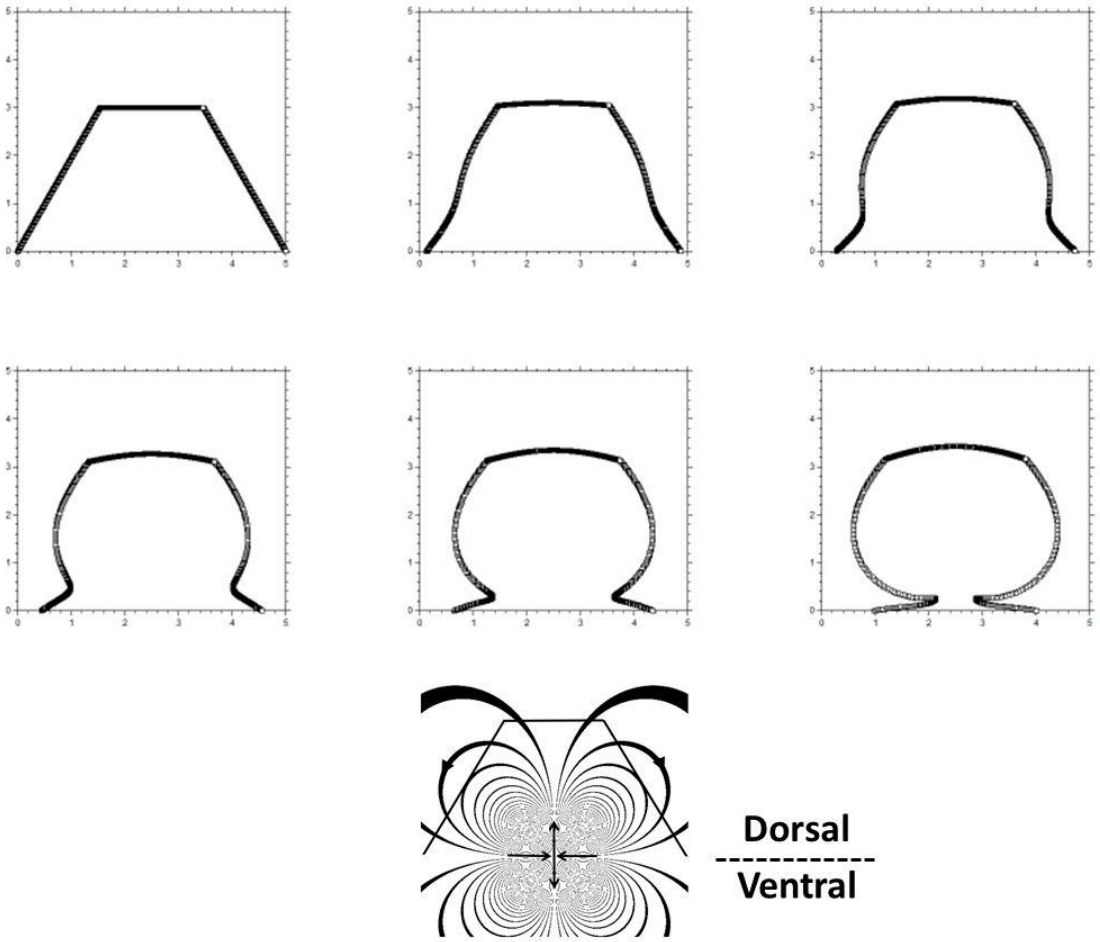

Figure 9A

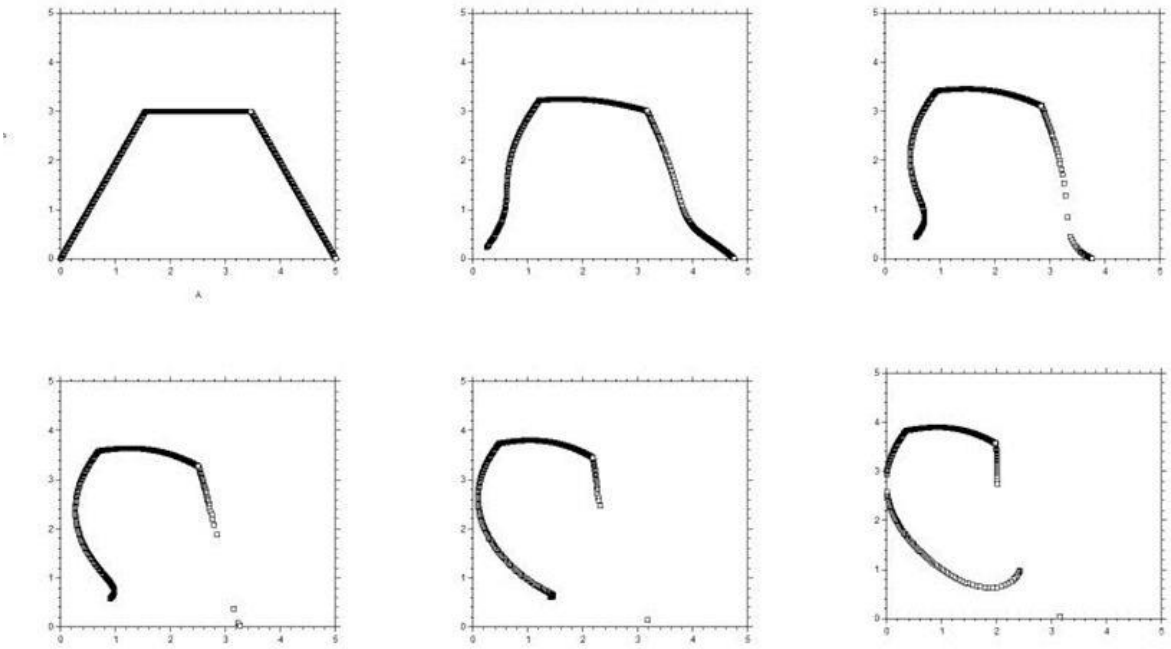

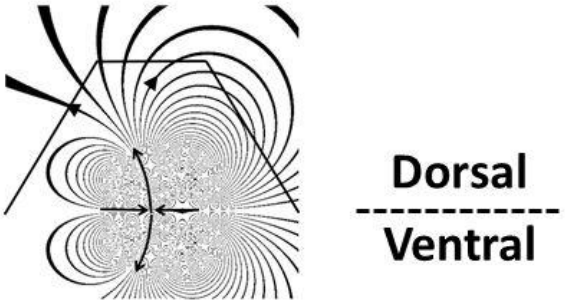

Figure 9B

Figure 9 Modelling of movements using the analytics developed in Ref. 8. We start with a truncated sector describing the otic territory (Fig. 9A), and assume a quadrupolar contraction along the horizontal axis at the DV boundary located at y=0. The flow is calculated analytically around four logarithmic vortices [8] forming a quadrupolar vortex flow. For the calculations in Fig. 9 a=2, c=3, b=1. For the calculation in Fig. 9A, $\alpha=\beta$, for the calculation in Fig. 9B $\beta=2\alpha$. The iso-$\Psi(x,y)$ map shows the associated streamline pattern. The trapezoidal kink progressively rounds off. Fig. 9B If we introduce an asymmetrical quadrupole we generate very simply conchoidal forms corresponding to ear patterns.

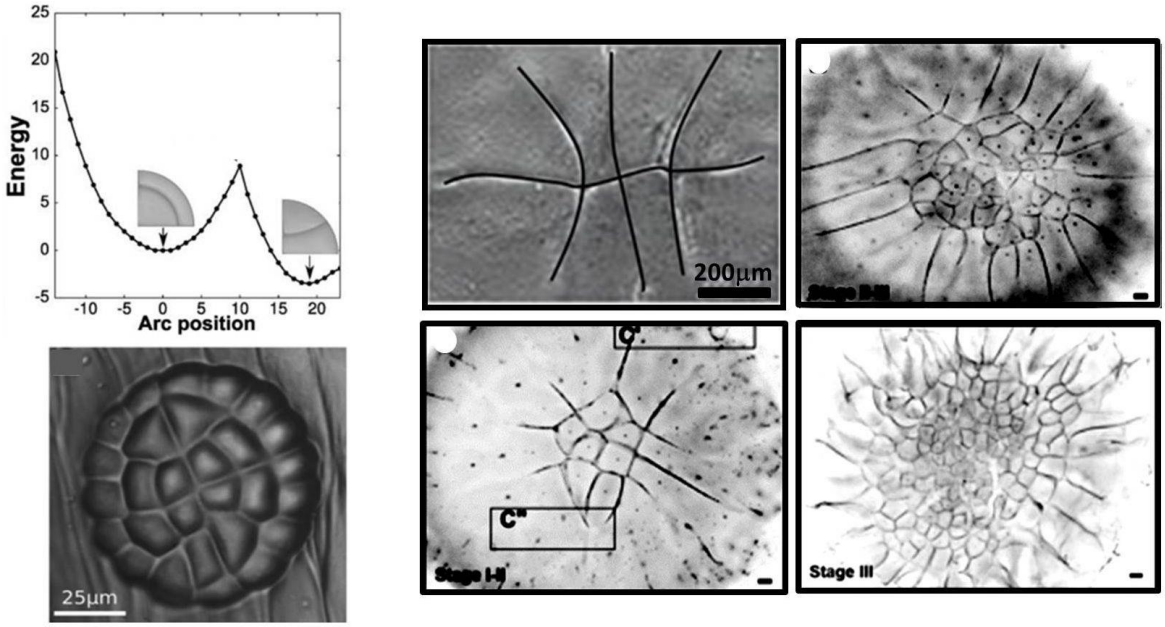
Energy
Arc position
25μm
200μm
Stage III

Figure 10A

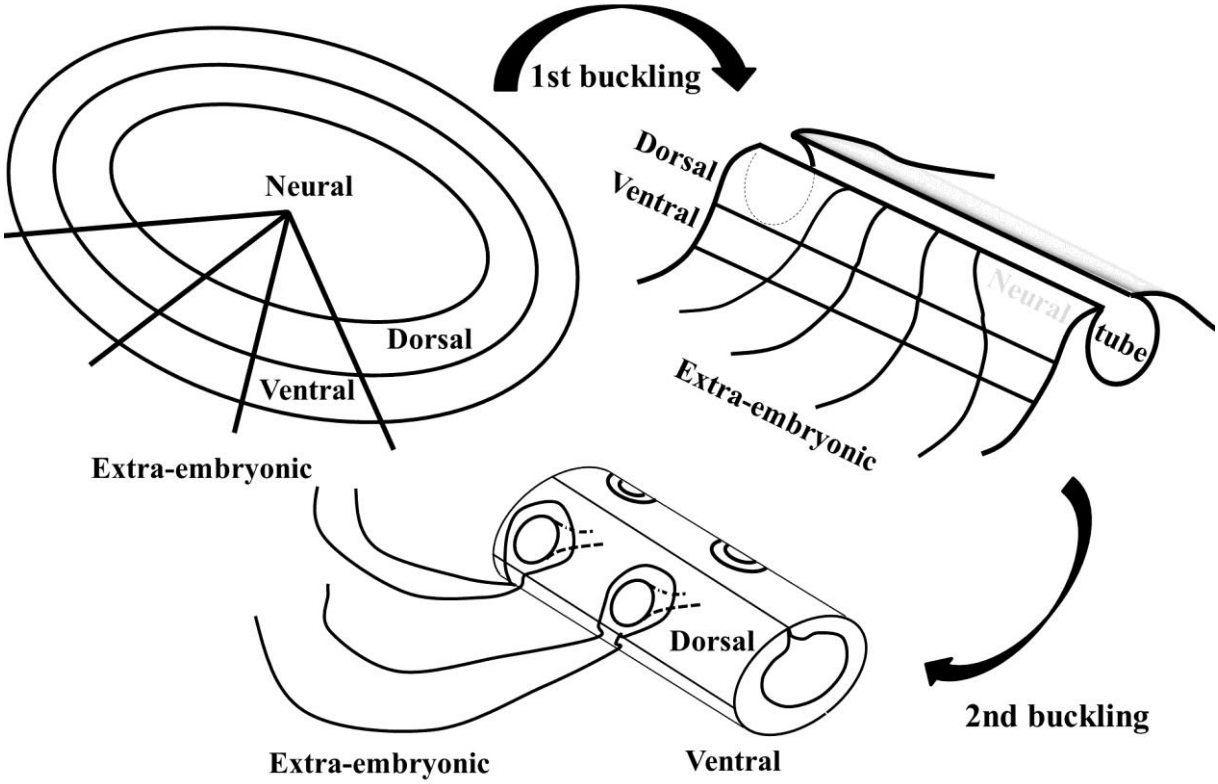
1st buckling
Neural
Dorsal
Ventral
Extra-embryonic
Dorsal
Ventral
Neural tube
Extra-embryonic
Dorsal
Extra-embryonic
Ventral
2nd buckling

Figure 10B

Figure 10 Fig. 10 A Top-Left : The origin of the structure in rings and sectors lies in the fact that radial cleavage is the most favorable, and orthoradial cleavage is the next most favorable cleavage (adapted from [24]). Bottom-Left : In plants the radial and orthoradial cleavages are very robust and conspicuous. Fig. 10A Right. Four stages of early cleavage in chicken, adapted from Refs. 20 and 21. In chicken, the first cleavages follow a pattern of radial and orthoradial cleavages which is arguably less conspicuous than in plants. Please note that the lines of third cleavage are nevertheless identical in Chicken and in *Dionaea Muscipula.* Fig. 10B A system of intersected rings and sectors undergoing biaxial tension and buckling will self deform into a system consisting of tubes inside tubes, decorated at right angles by tubular orifices diving down towards the neural tube.